Metal ablation by picosecond laser pulses: A hybrid simulation

Carsten Schäfer and Herbert M. Urbassek*
Fachbereich Physik, Universität Kaiserslautern, Erwin-Schrödinger-Straße, D-67663 Kaiserslautern, Germany

Leonid V. Zhigilei
Department of Materials Science and Engineering, University of Virginia, Charlottesville, Virginia 22903
(Received 8 September 2001; revised manuscript received 5 April 2002; published 5 September 2002)

We investigate picosecond laser ablation of metals using a hybrid simulation scheme. Laser energy input into the electron system and heat conduction within it are modeled using a finite-difference scheme for solving the heat conduction equation. Atom motion in the near-surface part (72 nm) of the sample is modeled using molecular dynamics. Energy transfer between the electronic and atomic subsystems due to electron-phonon coupling is taken into account. For the special case of 0.5 ps UV laser irradiation of copper, we investigate the fluence dependence of the ablation yield, the temperature and pressure evolution in the target, and the ablation mechanism.

DOI: 10.1103/PhysRevB.66.115404 PACS number(s): 79.20.Ds, 79.20.Ap, 61.80.Ba, 02.70.Ns

I. INTRODUCTION

Under intense laser irradiation, solid surfaces may emit atoms or clusters (droplets). This process—called ablation—is used in several applications, such as in laser modification of surfaces (drilling, cutting, surface patterning).[1] The emitted material is also used for a thin-film growth technique called pulsed laser deposition.[2] While previously, often conventional nanosecond lasers have been used for ablation, it has now become clear that ablation with ultrashort pulses—in the picosecond or femtosecond regime—is advantageous for several applications. Thus, in the case of metals with their large heat conductivity, picosecond pulses are reported[1] to give rise to well-reproducible ablation results, sharp cutting edges, and reduced droplet formation.

Laser light is absorbed in metals by the conduction-band electrons. After fast thermalization of the laser energy in the conduction band (within a few femtoseconds) electrons may quickly diffuse and thereby transport their energy deep into the target. At the same time, electrons transfer their energy to the target atoms; this process is controlled by the electron-phonon relaxation time, which is—strongly material dependent—in the order of a fraction of a picosecond to several tens of picoseconds. In consequence, the atoms heat up, and the lattice may melt and eventually undergo a phase transition to the supercritical liquid or gaseous state and ablate.

The conventional theoretical approach to laser ablation of metals is based on the so-called two-temperature model.[3] It is based on the coupled temperature evolution of the electronic and atomic subsystems. It has been used to describe satisfactorily the damage threshold, the melting of the material, and the size of the heat-affected zone.[4–6] However, it is only poorly suited to describing the ablation process proper: the latter is characterized by strong superheating, pressure effects, and the phase transition in the solid to a supercritical or gaseous state.[7,8] A modeling of these effects makes a more complete description of the atomic subsystem mandatory, which includes the equation of states, phase transition, and pressure effects.

In the present article, we base our description of the atomic system therefore on a molecular-dynamics simulation, in which all the above effects are inherently included. By coupling the molecular dynamics to the heat conduction equation for the electronic temperature, we obtain a hybrid simulation scheme which covers all necessary degrees of freedom characteristic for the laser ablation of metals. We use this simulation method to describe the 0.5 ps laser ablation of copper as a prototypical example.

II. METHOD

A. Heat conduction

We use a one-dimensional description of the laser ablation process, such as it applies at early times in the center of the laser focus, i.e., as long as lateral heat conduction can be neglected. We simulate the metal over a depth scale $L = 400$ nm. In an inner zone, extending from the surface at $x=0$ to a depth $l=72$ nm, we use a molecular-dynamics simulation to describe the atomic motion; cf. Fig. 1. In the

FIG. 1. Schematics showing the system and our solution scheme. The electronic system is simulated using a finite-difference scheme (FD). The laser irradiates at normal incidence and deposits energy in the electron system according to the source term $Q(x,t)$. The atomic system is treated by a molecular-dynamic scheme (MD) down to a depth $x=l$ and beyond that by a continuum approach (FD). Electronic and atomic systems are coupled by electron-phonon coupling.

rest of the system, $l<x<L$, we describe the atomic system using the heat conduction equation for the atomic temperature T_a,

$$C_a \frac{\partial T_a}{\partial t} = g(T_e - T_a). \tag{1}$$

The electron system is described over the whole simulation volume $0<x<L$ by a heat conduction equation for the electron temperature T_e,

$$C_e \frac{\partial T_e}{\partial t} = \frac{\partial}{\partial x}\Lambda_e \frac{\partial T_e}{\partial x} - g(T_e - T_a) + Q(x,t). \tag{2}$$

Here, C_e (C_a) denotes the specific heat and Λ_e (Λ_a) the heat conductivity of the electron (atom) system. The coefficient g embodies the coupling between the two subsystems by the electron-phonon coupling. Equations (1) and (2) are identical to the two-temperature model.[3] The source term

$$Q(x,t) = \frac{\Phi_a}{\tau}\frac{1}{\lambda} e^{-x/\lambda}, \quad 0<t<\tau, \tag{3}$$

represents the laser energy deposition into the electron system. Here, λ denotes the laser penetration depth, τ the laser pulse length, and

$$\Phi_a = (1-R)\Phi \tag{4}$$

the laser intensity *absorbed* in the target. Here Φ is the (nominal) laser intensity, and R is the target reflection coefficient. We assume the laser to irradiate at normal incidence.

In the present paper, we shall concentrate on copper as the target material. Here, the laser penetration depth $\lambda = 14$ nm is rather independent of the laser wavelength between 10 μm and 250 nm.[1] We shall fix the laser pulse duration $\tau = 0.5$ ps since experimental ablation data[9,10] are available here. Laser fluences Φ in the regime between 100 and 450 mJ/cm^2 will be investigated. Under these fluences, the reflection coefficient has been assumed as $R = 0.6$.[9]

The specific heat data of copper are taken as $C_e = \gamma T_e$, $\gamma = 96.6$ J/m^3 K^2, and $C_a = 3.5\times 10^6$ J/m^3 K. Literature values[6,11–14] on g vary between 0.1 and 2×10^{17} W/K m^3; however, in a recent compilation,[15] the value used by us, 1×10^{17} W/K m^3, has been adopted as the most reliable value.

The coefficient of the electron heat conductivity, $\Lambda_e(T_e, T_a)$, is subject to considerable uncertainty, since it depends on the local electronic and atomic temperatures. We implemented the functional form[4]

$$\Lambda_e = \alpha \frac{(\theta_e^2 + 0.16)^{5/4}(\theta_e^2 + 0.44)\theta_e}{(\theta_e^2 + 0.092)^{1/2}(\theta_e^2 + \beta\theta_a)}, \tag{5}$$

where $\theta_a = T_a/T_F$, $\theta_e = T_e/T_F$, and $T_F = 8.12\times 10^4$ K is the Fermi temperature of Cu. This expression has been argued to be valid over a wide range of temperatures, in particular also when T_e approaches (or exceeds) the Fermi temperature.[4] The two coefficients have been set to $\alpha = 377$ W/K m and $\beta = 0.139$ by the following procedure.

Expanding Eq. (5) for small temperatures we may compare to the well-known low-temperature expression[16]

$$\Lambda_e = \Lambda_0 \frac{bT_e}{aT_e^2 + bT_a}. \tag{6}$$

Here, $\Lambda_0 = \Lambda_e$ ($T_e = 300$ K, $T_a = 300$ K) is the electronic heat conductivity at room temperature, $\Lambda_0 = 400$ W/K m. The coefficients a and b describe electron-electron and electron-atom collision frequencies, respectively. Following the method of Ref. 16, they have been determined from the experimental data of Ref. 17 as $a = 1.75\times 10^7$ /s K^2, and $b = 1.98\times 10^{11}$ /s K. The comparison of the low-temperature behavior of Eqs. (5) and (6) gives the values of α and β quoted above.

Initially, at $t = 0$, the whole system is at 300 K. As boundary conditions for Eq. (2) we use energy-reflecting boundaries $\partial T/\partial x = 0$ at the ends of our simulation volume, $x = 0$ and $x = L$. These boundary conditions thus stipulate that electrons cannot give energy away to the vacuum above $x < 0$. Furthermore, these conditions allow for energy conservation as an easy check for the entire hybrid simulation; see below. They are realistic at $x = L$, since L has been chosen so large that there the temperature remains close to 300 K throughout the simulation. At $x = 0$, they are used here as a first approximation and will be further investigated in the future.

B. Molecular dynamics and coupling to electrons

The molecular-dynamics (MD) simulation is standard. We use a many-body interatomic interaction potential of the embedded-atom type.[18,19] We employ a (100) copper crystallite, which has been initially relaxed to 300 K. The simulation volume has a square lateral area of $A = 2.169 \times 2.169$ nm^2, containing 72 atoms per monolayer; its depth is 400 ML, i.e., 72 nm. By using laterally periodic boundary conditions, we can thus simulate the response of the material in the center of the laser spot. For a detailed study of phenomena that occur on a larger lateral space scale—such as the determination of the size distribution of droplet emission—the use of a broader simulation crystallite is necessary.[20]

Electronic energy is coupled to the atoms by adding a velocity-proportional force to the equation of motion of each atom.[21] Thus the equation of motion of atom i reads

$$M\frac{d^2\mathbf{r}_i}{dt^2} = -\nabla_{\mathbf{r}_i} V(\{\mathbf{r}_j\}) - \frac{g}{C_a}\frac{T_a - T_e}{T_a} M\frac{d\mathbf{r}_i}{dt}, \tag{7}$$

where V is the total potential energy of the atomic system as given by the many-body interaction potential and M is the atom mass. In the coupling term, the electron temperature T_e enters as calculated from Eq. (2).

The molecular-dynamics simulation also allows us to determine the local temperatures T_a, which are needed for solving the electron heat conduction equation, (2). To this end, we average the kinetic energies of all atoms in a cell.

We solve the heat conduction equations using a standard finite-difference scheme.[22] We found a cell width of 1 nm a convenient compromise between accuracy and computation speed.

At the deep end of the molecular-dynamics simulation, $x=l$, we use the so-called nonreflecting boundary conditions.[23] These have been developed in molecular-dynamics simulations of the laser ablation of organic materials,[20,24,25] and are necessary to prevent a reflection of the pressure wave traveling from the laser-irradiated surface inwards into the target. In short, this is achieved by matching the impedance of a boundary zone to the impedance of the MD volume; thus the boundary zone atoms respond to the passage of the pressure wave by letting it pass through the boundary without reflection. The wave is thus effectively absorbed. Without such a boundary condition, the pressure wave is reflected back towards the surface, leading to artifacts in the ablation behavior.[20]

We note that any possible effects of the boundary condition on the thermal energy in the system are confined within a depth of $\Delta x=\sqrt{2Dt}$ near the boundary. With a thermal diffusivity[26] of $D=1$ nm^2/ps and a duration of the simulation of $t=50$ ps, any such effect would be restricted to the lower 10 nm of the material and thus has no influence on the ablation behavior.

Molecular-dynamics simulations and the finite-difference scheme for the solution of the heat conduction equations work on different time scales. The time step for the molecular dynamics is around 1 fs, while that for the finite-difference scheme is taken smaller than $C_e(\Delta x)^2/(2\Lambda_e) \cong 36\times 10^{-18}$ s. We synchronize these two simulations by performing in each molecular-dynamics time step the necessary number of finite-difference time steps.

III. RESULTS

A. Energy dissipation in the metal

In the following, we shall first consider irradiation with $\Phi=170$ mJ/cm^2 intensity. We display the energy balance during the first 50 ps in the simulation in Fig. 2. Here we use a decomposition of the total energy $E_{\rm tot}$ in the hybrid simulation of the form

$$E_{\rm tot}=E_e+E_a^{MD}+E_a^{FD}=P(t), \tag{8}$$

where E_e is the energy of the electronic system, $E_a{}^{\rm MD}$ the atomic energy as calculated from the molecular dynamics—including kinetic and potential energy terms—and $E_a{}^{\rm FD}$ denotes the thermal energy of the atomic system in the region $l<x<L$; in all these contributions, the energy at $t=0$, i.e., corresponding to 300 K, has been subtracted. The time-accumulated energy input by the laser is denoted by

$$P(t)=\begin{cases} A\Phi_a\dfrac{t}{\tau}, & 0<t<\tau, \\ A\Phi_a, & t>\tau. \end{cases} \tag{9}$$

Figure 2 shows that we cannot achieve strict energy conservation, but observe fluctuations and energy loss in the order of 5%. This is due to the hybrid nature of our code and in particular to the (nonthermal part of the) energy of the pressure pulse propagating out from the MD zone; furthermore, we may have some energy loss due to the nonreflecting boundary conditions of the molecular-dynamics zone. We are confident that the small energy loss visible in Fig. 2 does not influence the ablation characteristics of our specimen.

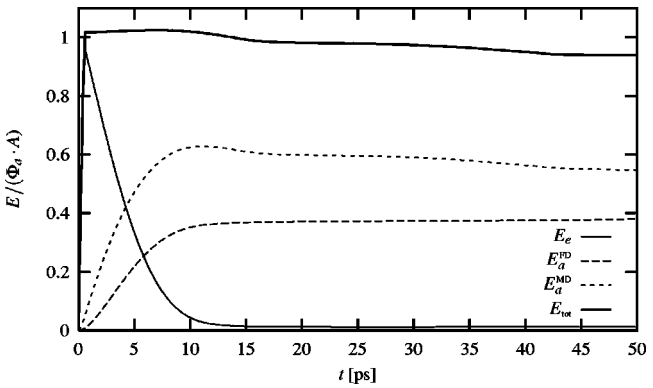

FIG. 2. Energy balance in the entire hybrid simulation, for a fluence of $\Phi=170$ mJ/cm^2. Energies are normalized to the total absorbed energy $\Phi_a A$. $E_{\rm tot}$: total energy. E_e: energy in electron system. $E_a^{\rm MD}$: energy in the atomic system, as calculated by molecular dynamics; here all kinetic and potential energies are taken into account. $E_a^{\rm FD}$: energies in the atomic system at a depth $l<x<L$ below the surface as calculated by the finite-difference scheme. In this plot, the energies of time $t=0$ have been subtracted.

Electrons deliver their energy to the atomic system with a time scale of around $\tau_{e\text{-}p}=7$ ps, as can be read off from the initially linear decay of the electron energy in Fig. 2. This time may be compared with the estimate $\gamma T_e/2g$, which is obtained from the heat conduction equation (2) for times $t>\tau$ by neglecting heat conduction and setting $T_e=25\,000$ K, the electron surface temperature at $t=\tau$; this estimate gives 12 ps. The larger part of the energy goes into the surface near zone $x<l$. Around 40% of the electron energy is converted to thermal atom motion deeper inside the target. We note that heat conduction of the atomic system plays only a rather minor role in this process; the energy found in the atomic system at depth $x>l$ has been deposited there by fast-diffusing electrons.

B. Time evolution of temperature and pressure

Figure 3 displays the (atomic) temperature and pressure distributions in the top 60 nm of the laser-irradiated material. Local temperatures have been calculated from the MD data as the local average of the atomic kinetic energies in a (local) center-of-mass system; analogously, pressures have been determined from the virial.[27] The temperature evolution shows a steady increase within 10 ps to the maximum temperature of about 1600 K. For comparison we note that the electron temperature reaches a maximum of $T_e=25\,000$ K immediately at the end of the laser pulse, $t=0.5$ ps. The atom temperature is quite homogeneous within the solid. The local fluctuations observed in the figure reflect the highly nonequilibrium state of the material under the energy density sup-

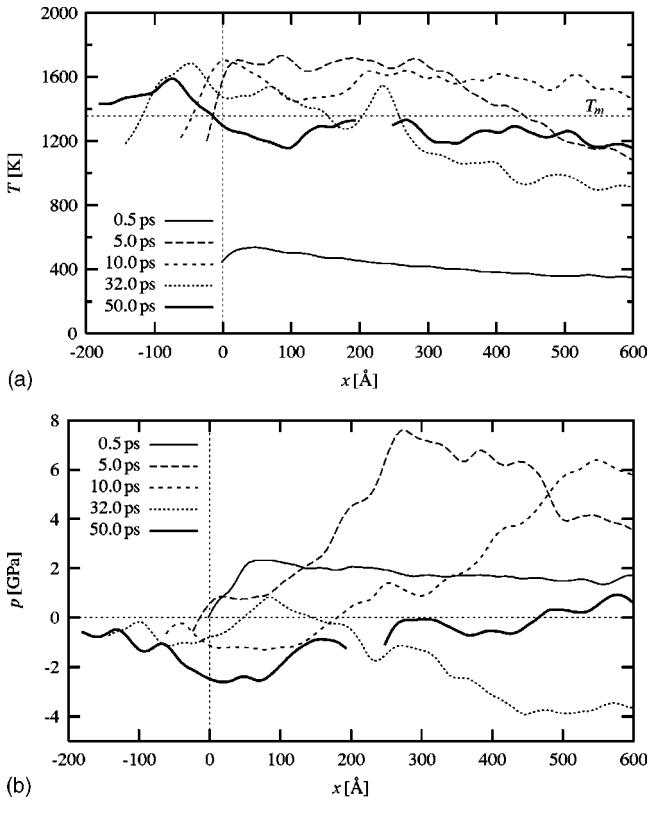

FIG. 3. Depth distribution of the temperature (a) and the pressure (b) at various times t after laser irradiation. The melting temperature of Cu, $T_m = 1358$ K, has been indicated. Positive pressure denotes compressive stress; negative values denote tensile stress. Gaps occur in the data (at $t = 50$ ps) where no material is present (after ablation).

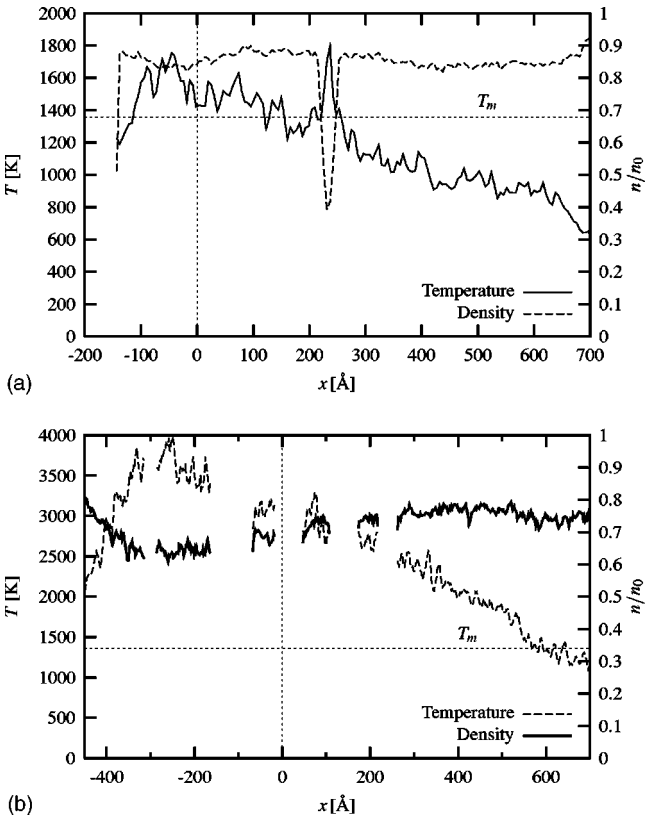

FIG. 4. Depth distribution of temperature and density: (a) for a laser fluence of 170 mJ/cm^2 at $t = 32$ ps, immediately after ablation occurred; (b) for a laser fluence of 400 mJ/cm^2 at $t = 35$ ps, where multiple spallation is visible. Density has been normalized to the solid-state density n_0. The melting temperature of Cu, $T_m = 1358$ K, has been indicated. Gaps occur in the data where no material is present (after ablation), i.e., where the vacuum separates the emitted large clusters.

plied by the laser and would only disappear after considerable spatial and temporal averaging. Note that, in particular, the laser penetration depth $\lambda = 14$ nm is irrelevant to the temperature profile. This is due to the swift electron diffusion, which completely smears out the laser energy deposition profile, Eq. (3). Note that due to the thermal expansion, the material expands out into the vacuum, into the region of negative x.

It is seen that at 10 ps the top 60 nm are above the melting temperature of Cu, $T_m = 1358$ K. However, an analysis of the snapshots from the simulations indicates that at 10 ps the melt zone extends only 20 nm down from the surface and, even at 30 ps, only to roughly 40 nm; the rest of the material became temporarily superheated without losing its crystalline structure. We note that superheating of metals has been observed in experiment[28,29] and also in previous MD simulations.[21]

In our simulation, melting, as a first-order phase transition, with its induced atomic disorder and the concomitant volume expansion [cf. also Fig. 4(a) below], starts at the surface and propagates into the crystal. This so-called *heterogeneous* melting process has been observed experimentally under fs laser irradiation of semiconductors like germanium[30] with melt-front velocities up to 10^3 m/s. A melt-front velocity of the order of $1-2\times10^3$ m/s can also be deduced from the data given above from our simulation. We are not aware of experimental measurements of the melt-front velocities in metals. The contrasting case of laser-induced *homogeneous* nucleation in the bulk of a superheated crystal does not appear to have been observed experimentally up to now. Theoretical reasoning advocates it to compete with heterogeneous melting only for superheating beyond 30%–50% of the melting temperature.[31]

The pressure is routinely calculated within the molecular-dynamics simulation from the virial; positive pressures denote compressive stress, negative pressures tensile stress. Figure 3(b) shows that a compression wave with maximum amplitudes on the order of 7 GPa travels into the solid. In its aftermath, a region of tensile stress follows. It reaches maximum stresses around -4 GPa. These stresses exceed the dynamic tensile strength of the material and lead to a tearing of the specimen (spallation).

C. Ablation

Figure 4(a) assembles the temperature and density profile at $t = 32$ ps after laser irradiation; this is about the time when ablation sets in, and a large cluster tears off at a depth of around 200 Å. The pressure distribution at this time was

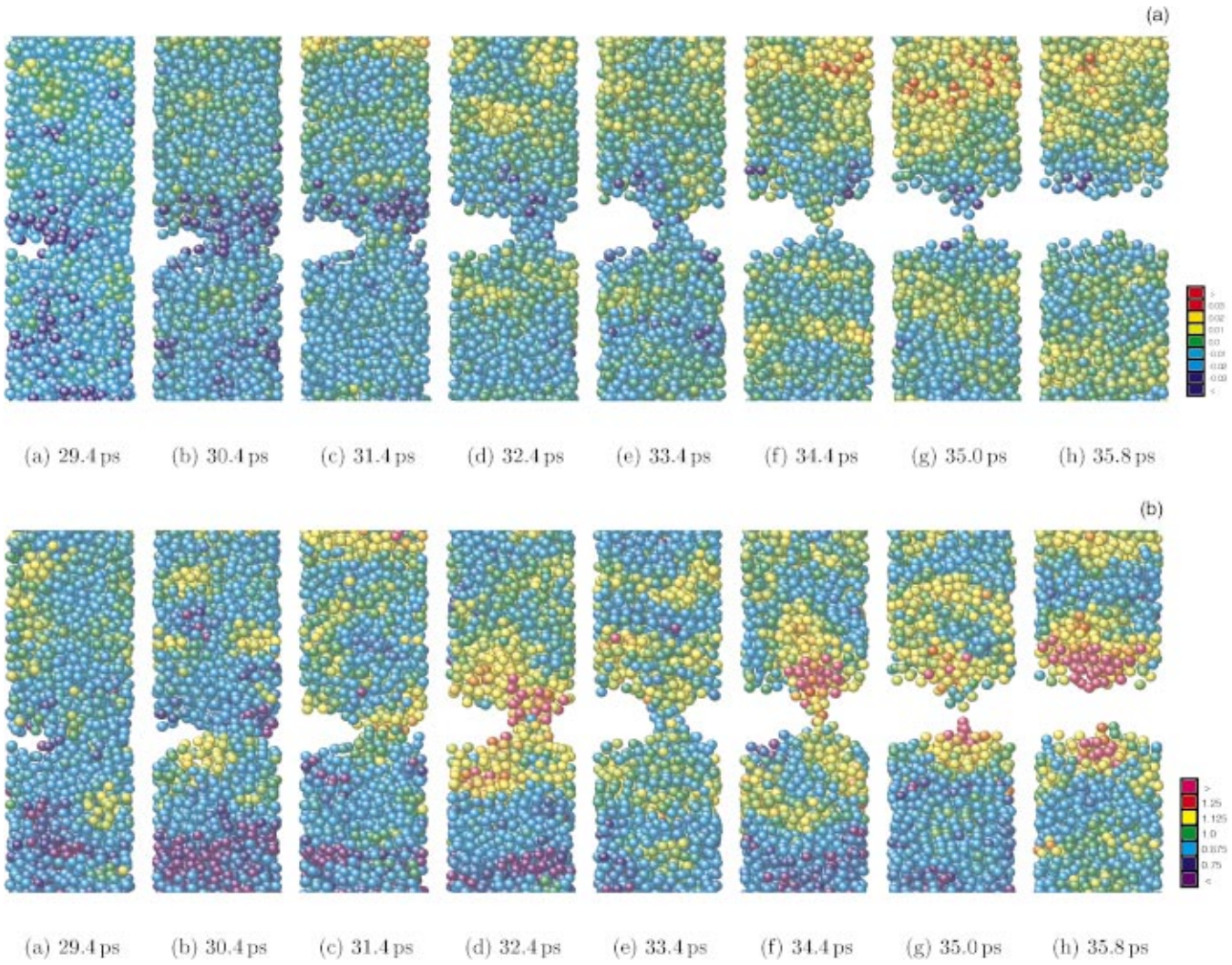

FIG. 5. (Color) Atomistic view of part of the laser-irradiated solid, at a time $t=32$ ps, immediately after ablation occurred. Cross sections through the simulation volume (height 60 Å, width 21 Å, thickness 10 Å) are shown at various times after laser irradiation. Atoms are colored (a) according to their local temperature, in units of the melting point of copper, $T_m=1358$ K, and (b) according to their local pressures, in units of the bulk modulus, $B=137$ GPa. The local temperature of an atom is defined as the average kinetic energy of all atoms around the central atom within a radius of 6.2 Å (cutoff of the interaction potential), in the center-of-mass system. Analogously, local pressures are defined as an average over the atomic virials.

included in Fig. 3. Temperature has its maximum close to the surface, but decreases inwards with a gradient of around 1 K/Å. The depth where spallation occurs is marked by a sharp decrease in density. At this point, a pronounced local tensile pressure develops (Fig. 3), while the temperature locally strongly increases. These features are characteristic of the spallation process, where the breaking of bonds leads to strong attractive forces (tensile pressure), while potential energy is converted to kinetic energy (heat). Due to the thermal expansion, melting, and the unloading of the pressure wave, the density in the surface near region has decreased to around 85% of the solid density, $n_0=0.081$ Å^{-3}. This compares well with the density of molten Cu, $0.89n_0$.[32] Note that the target material has expanded in this time out to around 140 Å; this corresponds to an average speed of 4–5 Å/ps.

Figure 5 gives an atomistic view of the irradiated solid during ablation. We see how a large cluster containing 12 000 atoms breaks free from the solid. The breakup occurs at a position where strong tensile pressures concentrate. This leads to a consecutive breaking of bonds between atoms, such that finally only a narrow bridge between the bulk material and the ablating cluster remains. The bridge is finally broken at around 35 ps. Note that as a consequence, a compressive wave travels away from the spallation point, which is well visible in the ejected cluster. The local production of heat is particularly pronounced when the small bridge between bulk and cluster tears. Then temperatures strongly exceeding the melting temperature arise. In the terminology of recent theoretical studies on the laser ablation of organic materials,[20] this ablation occurs in the so-called stress confinement regime. We note that ablation did not appear at the time when the tensile wave passes but rather in its aftermath.

Simulations performed for higher laser fluences Φ essentially follow the characteristics described above. We give a

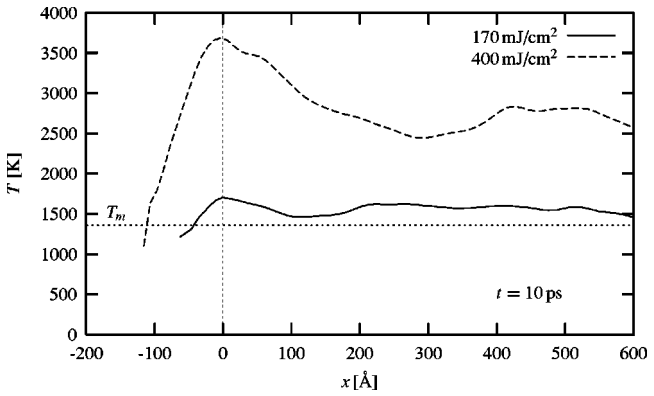

FIG. 6. Comparison of atomic temperatures in the solid at $t = 10$ ps after laser irradiation for $\Phi = 170$ and 400 mJ/cm^2 irradiation.

few quantitative details for 400 mJ/cm^2 irradiation. Here the maximum electron temperature at the surface amounts to 45 000 K. The maximum temperatures achieved in the atomic system are 4000 K, and the atomic temperatures spread out quite homogeneously inside the solid; cf. Fig. 6. Maximum pressures amount to $+14$ and -5 GPa. Ablation already sets in at 25 ps, but the solid tears at several points more or less simultaneously, as displayed in Fig. 4(b). This results in a higher ablation yield, 35 nm/pulse, and a distribution of clusters emitted rather than a single cluster. We note that our results for the large fluences need to be taken with some caution since the ablation depth is at 50% of our MD simulation volume.

D. Comparison to experiment

Figure 7 assembles the ablation yields for a series of simulations performed with varying laser intensities Φ on copper; each simulation lasted 50 ps. We observe a rather sharp ablation threshold of around 170 mJ/cm^2. This is in good agreement with the experimental data, which report a threshold fluence of 170 mJ/cm^2 for 0.5 ps ablation by a 248 nm laser[9] and 140 mJ/cm^2 for 0.15 ps laser at 780 nm.[10] As soon as ablation sets in, the ablation yield is rather constant, 24–30 nm/pulse. It only increases at fluences beyond 350 mJ/cm^2, where the yield doubles.

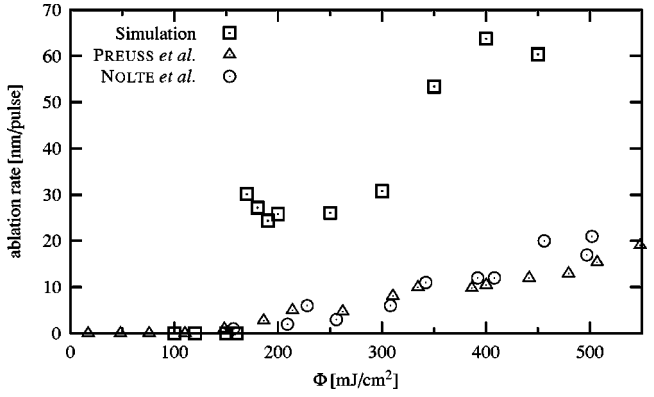

FIG. 7. Ablation yield vs fluence for 0.5 ps laser irradiation of copper. ○: experiment by Nolte *et al.* (Ref. 10), at a wavelength of 780 nm. △: experiment by Preuss *et al.* (Ref. 9) at a wavelength of 248 nm. □: simulation results.

At the fluences studied in this paper—at and slightly above the ablation threshold—we found spallation (or mechanical failure) to be the relevant ablation mechanism. As a consequence, the ablation products consist mainly of large chunks of matter or droplets rather than of monatomics or small clusters. This feature does not appear to have been reported in the literature. While energy spectra of emitted (monomeric) *ions* have been measured,[33–35] the analogous experimental determination of the *neutral* component, and in particular its mass distribution, still awaits measurement. We note, however, that Sokolowski-Tinten and co-workers[36–38] measured high-contrast optical interference patterns (Newton rings) after fs laser ablation of both semiconductors and metals at fluences comparable to those of our study. These patterns were interpreted to be due to a highly coherent emission of the ablated material; they are thus compatible with the coherent emission mechanism (spallation) reported in the present study.

A quantitative comparison to experimental data shows that our yields are a factor of between 3 and 5 too high. This may be due to the fact that experimental data were taken as an average over many laser shots; for example, Nolte *et al.*[10] report that they took the measurement after several hundred pulses which were shot at a frequency of 1 kHz at the target. These authors also report that they observe a decrease in the ablation yield for a larger number of shots. In contrast, our simulation pertains to a single shot to a well-defined crystalline surface. The irradiation-induced surface modification may change the optical parameters of the specimen and, hence, the absorption.

IV. DISCUSSION: MECHANISM OF ABLATION

As we can see from the snapshots given in Fig. 5, the material ejection in the simulation proceeds through the separation of a large surface layer of material, ~ 20 nm in size, from the bulk of the irradiated sample. A similar process of material ejection has been previously observed in MD simulations of the laser ablation of molecular systems and has been attributed to the photomechanical effects caused by laser-induced stresses.[20,25,39] It has been discussed that the magnitude of the laser-induced stresses and the role of the associated photomechanical effects in the material removal become significant when the time of the laser pulse duration, τ, is shorter than the time of mechanical equilibration of the absorbing volume, τ_s.[20] This condition, termed inertial or stress confinement, can be expressed as $\tau \leqslant \tau_s \sim L_p/c$, where c is the speed of sound in the irradiated material and L_p is the characteristic length of the laser energy deposition. In the case of a metal target irradiated with a sub-ps laser pulse, the relevant parameters are not the laser pulse duration and the optical penetration depth, but the time and length scales of the energy transfer from the electronic subsystem to the thermal energy of atomic vibrations. These scales are defined by the electronic heat conductivity and the strength of the electron-phonon coupling. For the system

considered in the present work, we can estimate the time of the equilibration to be $\tau_{e\text{-}p} \sim 7$ ps and the characteristic size of the heated region to be $L_p \sim 100$ nm. The time needed for relaxation of the laser-induced thermoelastic stress can be then estimated as $\tau_s \sim L_p/c = 19$ ps. Here the value $c = 54$ Å/ps has been used which has been measured in the simulation to apply under our conditions of laser irradiation; c is larger than the speed of sound in the [100] direction in Cu, $c = 44$ Å/ps. Thus the condition for the stress confinement is satisfied, as $\tau_{e\text{-}p} \leqslant \tau_s$.

Under stress confinement the lattice temperature increase proceeds under nearly constant volume conditions, leading to the buildup of high compressive thermoelastic pressure. The pressure buildup can be seen in Fig. 3(b), where the spatial distribution of the local hydrostatic pressure in the irradiated sample is shown for different times. A maximum compressive pressure as high as 7 GPa is reached below the surface a few ps after the end of the laser pulse. In Fig. 3(b) we see that at 5 ps the compressive pressure follows the temperature profile in the bulk of the sample and is decreasing near the surface due to the onset of an unloading pressure wave. The unloading wave that propagates from the surface of the sample leads to the development of tensile stress, which is increasing with depth under the surface. In the case of the elastic material response, the tensile component would increase with depth and would reach a maximum value equal to the compressive component at approximately the length of the atomic temperature increase. In the simulations performed at laser fluences above the ablation threshold fluence, however, the tensile pressure exceeds the dynamic tensile strength of the material and causes mechanical fracture or spallation. The amplitude of the tensile component of the pressure wave is determined in this case by the dynamic tensile strength of the material and can be significantly lower than the amplitude of the compressive component. In particular, for the simulation performed at a laser fluence of 170 mJ/cm^2, a maximum tensile pressure of -4 GPa has been reached at a depth of ~ 20 nm under the surface, causing the spallation and ejection of a layer or cluster of material, as shown in Fig. 5. Although the tensile component of the pressure wave becomes even higher as the wave propagates into the sample, it does not cause spallation or visible damage deeper in the sample.

Similar observations have been reported for organic materials, where the position of the spallation plane is found to be located closer to the surface as compared to the depth where maximum tensile stress is reached.[20,39] This observation has been attributed to the strong temperature dependence of the ability of the material to support tensile stresses.[20,39] The tensile strength of the material heated by the laser irradiation decreases significantly as the temperature increases. The depth of the photomechanical damage is determined therefore by the balance between the tensile pressure that is increasing with depth and the decreasing thermal softening due to the laser heating. In simulations performed with higher laser fluences spallation at multiple spallation planes is observed, reflecting the higher thermoelastic pressure and the high temperature of the surface region. Note that since the mechanical stability of the surface region is strongly affected by the laser heating, analytical predictions on the depth of the spallation planes that are based only on the analysis of the thermoelastic response of the heated material[40] cannot be directly applied for the quantitative description of the simulation results.

V. CONCLUSIONS

We performed a hybrid simulation to study picoseond laser ablation of metals. A finite-difference scheme implements the two-temperature model, incorporating laser energy absorption into the electronic system and fast electron diffusion. A molecular-dynamics simulation models atomistically the processes in a surface near zone, including naturally pressure effects, phase transitions, and other equation-of-state effects.

Ablation is triggered by the passage of the unloading wave, which follows the inwards traveling compression wave induced by the thermal expansion of the irradiated material. Tensile stresses of 4 GPa are reached in the example of 170 mJ/cm^2, 0.5 ps laser irradiation of copper. Ablation occurs by the breakage (spallation) of the target at a depth of around 20 nm. The ablation threshold is at 170 mJ/cm^2, in good agreement with experiment. The ablation rate is by a factor of 3–5 higher than in the experiments. At intensities 2 times the ablation threshold, the ablation yield strongly increases by the process of multiple spallation. This mechanism is characteristic of the so-called stress confinement regime of laser ablation.

ACKNOWLEDGMENTS

The authors are grateful to G. Betz and S. Nolte for discussions on several aspects of this work. They thank the computer center RHRK, University of Kaiserslautern, for making available computer time for this study.

*Electronic address: urbassek@rhrk.uni-kl.de; URL: http://www.physik.uni-kl.de/urbassek/

[1] D. Bäuerle, *Laser Processing and Chemistry*, 3rd ed. (Springer, Berlin, 2000).

[2] *Pulsed Laser Deposition of Thin Films*, edited by D.B. Chrisey and G.K. Hubler (Wiley, New York, 1994).

[3] S.I. Anisimov, B.L. Kapeliovich, and T.L. Perel'man, Sov. Phys. JETP **39**, 375 (1974).

[4] S.I. Anisimov and B. Rethfeld, Izv. Ross. Akad. Nauk, Ser. Fiz. **61**, 1642 (1997).

[5] J. Hohlfeld, S.-S. Wellershoff, J. Güdde, U. Conrad, V. Jähnke, and E. Matthias, Chem. Phys. **251**, 237 (2000).

[6] P.B. Corkum, F. Brunel, N.K. Sherman, and T. Srinivasan-Rao, Phys. Rev. Lett. **61**, 2886 (1988).

[7] R. Kelly and A. Miotello, Nucl. Instrum. Methods Phys. Res. B **122**, 374 (1997).

[8] A. Miotello and R. Kelly, Appl. Phys. A: Mater. Sci. Process. Suppl. **69**, S67 (1999).

[9] S. Preuss, A. Demchuk, and M. Stuke, Appl. Phys. A: Mater. Sci. Process. **61**, 33 (1995).
[10] S. Nolte, C. Momma, H. Jacobs, A. Tünnermann, B.N. Chichlov, B. Wellegehausen, and H. Welling, J. Opt. Soc. Am. B **14**, 2716 (1997).
[11] H.E. Elsayed-Ali, T.B. Norris, M.A. Pessot, and G.A. Mourou, Phys. Rev. Lett. **58**, 1212 (1987).
[12] G.L. Eesley, Phys. Rev. Lett. **51**, 2140 (1983).
[13] Z.G. Wang, C. Dufour, E. Paumier, and M. Toulemonde, J. Phys.: Condens. Matter **6**, 6733 (1994).
[14] S.D. Brorson, A. Kazeroonian, J.S. Moodera, D.W. Face, T.K. Cheng, E.P. Ippen, M.S. Dresselhaus, and G. Dresselhaus, Phys. Rev. Lett. **64**, 2172 (1990).
[15] M. Bonn, D.N. Denzler, S. Funk, M. Wolf, S.-S. Wellershoff, and J. Hohlfeld, Phys. Rev. B **61**, 1101 (2000).
[16] X.Y. Wang, D.M. Riffe, Y.-S. Lee, and M.C. Downer, Phys. Rev. B **50**, 8016 (1994).
[17] M. Kaveh and N. Wiser, Adv. Phys. **33**, 257 (1984).
[18] H. Gades and H.M. Urbassek, Nucl. Instrum. Methods Phys. Res. B **69**, 232 (1992).
[19] M.S. Daw, S.M. Foiles, and M. Baskes, Mater. Sci. Rep. **9**, 251 (1993).
[20] L.V. Zhigilei and B.J. Garrison, J. Appl. Phys. **88**, 1281 (2000).
[21] H. Häkkinen and U. Landman, Phys. Rev. Lett. **71**, 1023 (1993).
[22] W.H. Press, B.P. Flannery, S.A. Teukolsky, and W.T. Vetterling, *Numerical Recipes* (Cambridge University Press, Cambridge, England 1989).
[23] L.V. Zhigilei and B.J. Garrison, in *Multiscale Modeling of Materials*, edited by T. Diaz de la Rubia, T. Kaxiras, V. Balatov, N. M. Ghoniem, and R. Phillips, Mater. Res. Soc. Symp. Proc. Proceeding No. **538** Material Research Society, Pittsburgh, 1999, p.491.
[24] L.V. Zhigilei and B.J. Garrison, Proc. SPIE **3254**, 135 (1998).
[25] L.V. Zhigilei and B.J. Garrison, in *Proceedings of the International Conference on Modeling and Simulation of Microsystems, Semiconductors, Sensors, and Actuators (MSM'99)*, (Computational Publications, Boston, 1999), p. 65. Online http://nanotech2003.comlprocs/MSM99131M21.05
[26] G. Leibfried, *Bestrahlungseffekte in Festkörpern* (Teubner, Stuttgart, 1965).
[27] T.J. Colla and H.M. Urbassek, Radiat. Eff. Defects Solids **142**, 439 (1997).
[28] J. Daeges, H. Gleiter, and J.H. Perepezko, Phys. Lett. A **119**, 79 (1986).
[29] L. Grabak, J. Bohr, H.H. Andersen, A. Johansen, E. Johnson, L. Sarholt-Kristensen, and I.K. Robinson, Phys. Rev. B **45**, 2628 (1992).
[30] K. Sokolowski-Tinten, C. Blome, C. Dietrich, A. Tarasevitch, M. Horn-von-Hoegen, D. von der Linde, A. Cavalleri, J. Squier, and M. Kammler, Phys. Rev. Lett. **87**, 225701 (2001).
[31] B. Rethfeld, K. Sokolowski-Tinten, D. von der Linde, and S.I. Anisimov, Phys. Rev. B **65**, 092103 (2002).
[32] *Zahlenwerte und Funktionen*, edited by H. Borchers and E. Schmidt, Landolt-Börnstein, Vol. IV, pt. 2b (Springer, Berlin, 1964), p. 672.
[33] P.A. Van Rompay, M. Nantel, and P.P. Pronko, Appl. Surf. Sci. **127-129**, 1023 (1998).
[34] S. Amoruso, X. Wang, C. Altucci, C. de Lisio, M. Armenante, R. Bruzzese, and R. Velotta, Appl. Phys. Lett. **77**, 3728 (2000).
[35] M. Ye and C.P. Grigoropoulos, J. Appl. Phys. **89**, 5183 (2001).
[36] K. Sokolowski-Tinten, J. Bialkowski, A. Cavalleri, D. von der Linde, A. Oparin, J. Meyer-ter-Vehn, and S.I. Anisimov, Phys. Rev. Lett. **81**, 224 (1998).
[37] K. Sokolowski-Tinten, J. Bialkowski, M. Boing, A. Cavalleri, and D. von der Linde, Phys. Rev. B **58**, R11 805 (1998).
[38] A. Cavalleri, K. Sokolowski-Tinten, J. Bialkowski, M. Schreiner, and D. von der Linde, J. Appl. Phys. **85**, 3301 (1999).
[39] A.G. Zhidkov, L.V. Zhigilei, A. Sasaki, and T. Tajima, Appl. Phys. A: Mater. Sci. Process. **73**, 741 (2001).
[40] R.S. Dingus and R.J. Scammon, Proc. SPIE **1427**, 45 (1991).